# 87. EHT Model Studies on Coordination-Sphere Effects in the Elementary Steps of d⁰ Transition-Metal-Catalyzed *Ziegler-Natta* Polymerization

by **Roland Mohr**[a]), **Heinz Berke**[b])*, and **Gerhard Erker**[a])

[a]) Organisch-chemisches Institut, Universität Münster, Orleansring 23, D-W-4400 Münster
[b]) Anorganisch-chemisches Institut, Universität Zürich-Irchel, Winterthurerstr. 190, CH–8057 Zürich
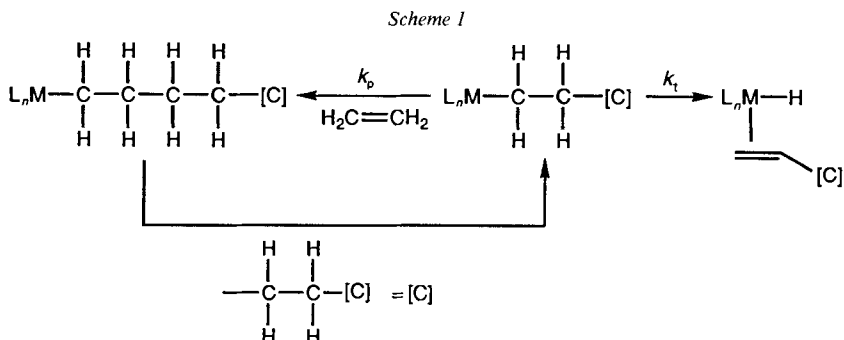
In a theoretical investigation on *Ziegler-Natta* catalysis, the influence of the coordination number and ligand type of model compounds in relevant reaction steps were studied. Thus, by using the MEHT method, insertion reactions of ethylene into $Zr–CH_3$ and $Zr–H$ bonds were analyzed in systems of the type $[Zr(C_2H_4)R_4R']^-$ $[Zr(Cp)(C_2H_4)R_2R']$, and $[Zr(Cp)(C_2H_4)R_3R']^-$ (R=R'=CH_3, R=CH_3, R'=H). It was found that all processes do not have significant kinetic barriers, whereas the reverse reactions in particular the $\beta$-hydride elimination have relatively high ones. The influence of coordination geometry and number on these transformations was found to be insignificant. While studying related conversions starting from $[Zr(L)(C_2H_4)R_3R']$, $[Zr(Cp)(C_2H_4)RR'(L)]^+$, and $[Zr(Cp)(C_2H_4)R_2R'(L)]$ (L = $\pi$-donor, R=R'=CH_3 or R=CH_3, R'=H) compounds a pronounced $\pi$-donor effect was observed. Methyl insertions in these cases showed a higher computed activation barrier than hydride migrations. An orbital basis for this phenomenon was provided and conclusions concerning chain-length control in *Ziegler-Natta* catalysis were drawn.

**Introduction.** – Recent academic and industrial interest in *Ziegler-Natta* catalysis has focussed on the regio- and stereoselectivity of polymerization reactions of substituted $\alpha$-olefins [1a, b]. Similar efforts were dedicated to studies concerning the control of the average molecular-weight distribution of the obtained polymer [1c, d]. While the earlier aspect has been addressed by the application of appropriate topochemical models [2], the question of which factors determine the chain length seems to be dependent predominantly on electronic conditions [3]. Up to now, this point has attracted only scant attention, and it is the goal of this paper to provide more insight into the electronic prerequisites of the *Ziegler-Natta* catalysis.

For any kind of electronic analysis of complex chemical-reaction systems, it is essential to acquire basic knowledge of its important elementary steps. Taking the *Cossee* mechanism [4] as a first-order approximation for the description of *Ziegler-Natta* catalysis, the degree of olefin polymerization has been rationalized in terms of a competition between two reaction branches: chain propagation (olefin addition, alkyl migration) $k_p$ and chain termination ($\beta$-hydride elimination, olefin elimination) $k_t$ [5][1]. Any influence on *Ziegler-Natta* catalysis may primarily operate *via* the setting of the $k_p/k_t$ ratio (*Scheme 1*).

It should be noted, that the kinetics behind $k_p$ and $k_t$ in *Scheme 1* are to be considered as a sum of elementary steps, in which, however, the olefin complexation or decomplexation are normally of minor importance. Thus, the $k_p/k_t$ ratio should more or less be

---

[1])    For other mechanistic pathways taken in chain termination, *e.g.* $\beta$-alkyl elimination, see [5c–e].

*Scheme 1*

$$L_nM-\overset{\overset{H}{|}}{\underset{\underset{H}{|}}{C}}-\overset{\overset{H}{|}}{\underset{\underset{H}{|}}{C}}-\overset{\overset{H}{|}}{\underset{\underset{H}{|}}{C}}-\overset{\overset{H}{|}}{\underset{\underset{H}{|}}{C}}-[C] \xleftarrow[H_2C=CH_2]{k_p} L_nM-\overset{\overset{H}{|}}{\underset{\underset{H}{|}}{C}}-\overset{\overset{H}{|}}{\underset{\underset{H}{|}}{C}}-[C] \xrightarrow{k_t} L_nM-H$$

$$-\overset{\overset{H}{|}}{\underset{\underset{H}{|}}{C}}-\overset{\overset{H}{|}}{\underset{\underset{H}{|}}{C}}-[C] \quad =[C]$$

characterized by the ratio of $\beta$-alkyl migration/$\beta$-hydride elimination, especially, when only electronic effects are considered. From a general point of view, $\beta$-alkyl migration and $\beta$-hydride elimination are related to each other representing either forward or reverse reaction, since both constitute 1,3-shift-type processes with very similar (isolobal) migrating groups (*Scheme 2*).

*Scheme 2*
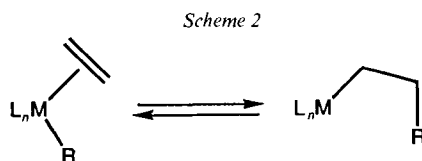
R = alkyl, H

In the case of early-transition-metal catalysis, one normally deals with the situation of $k_t \ll k_p$ leading to high-average-molecular-weight polymer. The case of $k_t \approx k_p$ which affords oligomers is more typical for late-transition-metal elements [6], but many examples are known where certain ligand-substitution patterns generate this selectivity with Group-IVb transition-metal catalysts as well [7]. The fundamental relations between the type of coordination sphere and the chain length are still elusive and no systematic methodology has yet emerged.

Trying to understand the basic factors controlling the $k_p/k_t$ ratio, we undertook a theoretical analysis aimed at revealing the role of the general electronic features which determine the competition constant of these 1,3-shift reactions. We set out to study the influence of the metal coordination number represented by specific types of coordination spheres. On the other hand, it seemed interesting to probe individual ligand effects on this parameter.

**Results and Discussions.** – For our computational analysis, we chose three different types of Zr-based model substrates. We started with a geometry optimization of the octahedral complexes **1–3**, the formally seven-coordinated species **4–6**, and the eight-coordinated compounds **7–12** (in this view a Cp⁻ ligand formally occupies three polyhedral positions, since it behaves electronically as tridentate [8]).

The octahedral systems **1–3** were selected as starting molecules because of their topological resemblance to the proposed *Ziegler-Natta* intermediates of the *Cossee* type [4]. Half-sandwich complexes of type **4–6** seemed to be quite realistic models of existing seven-coordinated early-transition-metal compounds, and some representatives of this
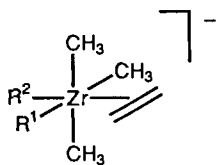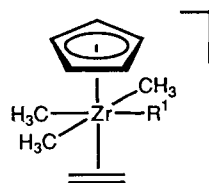
1 $R^1 = R^2 = CH_3$
2 $R^1 = H, R^2 = CH_3$
3 $R^1 = CH_3, R^2 = H$
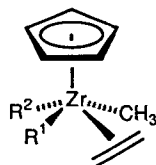
4 $R^1 = R^2 = CH_3$
5 $R^1 = H, R^2 = CH_3$
6 $R^1 = CH_3, R^2 = H$
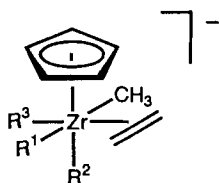
7 $R^1 = R^2 = R^3 = CH_3$
8 $R^1 = H, R^2 = R^3 = CH_3$
9 $R^2 = H, R^1 = R^3 = CH_3$
10 $R^3 = H, R^1 = R^2 = CH_3$

11 $R^1 = CH_3$
12 $R^1 = H$

class of complexes are in their basic structural features comparable to suggested intermediates of ethylene-polymerization catalysis [3] [9]. Compounds **7–12** represent alkylated derivatives of known eight-coordinated Zr complexes [10]. They were included in our investigations as hypothetical species, since they nicely complete the series of the model compounds with increasing coordination number. In addition they are mono($\eta$-cyclopentadienyl)zirconium complexes, the catalytic importance of which to some extent has been explored experimentally [11].

Concerning the actual polymerization-catalysts complexes **1–12** may despite some resemblance in structural properties still be viewed at as rather artificial representatives. They might in fact have nothing in common with any existing real catalytic species. However, this work is designed to provide insight into the mentioned general aspects of the elementary steps of such catalytic conversions. For the elucidation of such features, even quite simplified and restricted models should nevertheless suffice. Compounds **1–12** display a prominent common topological element: their structures contain a square plane of ligands, in which the migrating group and its target, the olefin, are located. In the later context, it will be seen that this feature gives rise to a great deal of similarities of the insertion processes under consideration.

Compounds **2** and **3**, **5**, and **6**, and **8–12** are geometrical isomers, respectively. To test the reliability of the chosen calculational procedure, the MEHT method [12], at these specific systems and to judge the importance of geometrical isomerism in these types of compounds, all possible isomers were optimized with regard to their essential geometrical parameters (see *Appendix*, and for the EH parameters used see *Table 7* there).

Table 1. *Computed Total Energies* [eV] *Optimized Bond Distances from the Zr-Centers* [Å], *$CH_2=CH_2$ Separations, and 'Equatorial' Bond Angles around* [°]

| | E | Zr–Cp [a] | Zr–CH$_3$ | Zr–C$_2$H$_4$ [e] | Zr–R$^1$ | CH$_2$=CH$_2$ | R$^1$–Zr–C$_2$H$_4$ [g][f] | R$^1$–Zr–R$^2$ [g] | R$^2$–Zr–CH$_3$ [g] | CH$_3$–Zr–C$_2$H$_4$ [g][f] |
|---|---|---|---|---|---|---|---|---|---|---|
| **1** | – 909.10 | 2.18[b] | 2.21 | 2.55 | 2.18[d] | 1.49 | 102 | 78 | 78 | 102 |
| **2** | – 801.75 | 2.27[b] | 2.20 | 2.45 | 1.58[c] | 1.49 | 88 | 71 | 76 | 124 |
| **3** | – 801.90 | 2.18[b] | 2.23 | 2.45 | 1.58[c] | 1.50 | 107 | 71 | 71 | 107 |
| **4** | –1093.38 | 1.98 | 2.17 | 2.62 | 2.17[d] | 1.50 | 86 | 81 | 81 | 86 |
| **5** | – 986.57 | 1.92 | 2.16 | 2.55 | 1.57[c] | 1.47 | 85 | 72 | 81 | 88 |
| **6** | – 986.75 | 1.92 | 2.19 | 2.57 | 2.19[d] | 1.49 | 93 | 71 | 71 | 93 |
| **7** | –1231.16 | 2.01 | 2.28 | 2.87 | 2.26[d] | 1.51 | 91 | 78 | 78 | 91 |
| **8** | –1124.18 | 1.99 | 2.32 | 2.75 | 1.58[c] | 1.50 | 84 | 70 | 81 | 111 |
| **9** | –1124.46 | 1.97 | 2.26 | 2.73 | 1.56[c] | 1.49 | 82 | 86 | 86 | 82 |
| **10** | –1124.33 | 2.01 | 2.31 | 2.63 | 1.58[c] | 1.49 | 103 | 70 | 70 | 103 |
| **11** | –1230.87 | 2.07 | 2.21 | 3.17 | 2.18[d] | 1.47 | 87 | 88 | 87 | 88 |
| **12** | –1123.80 | 2.03 | 2.22 | 2.75 | 1.58[c] | 1.50 | 82 | 91 | 91 | 82 |

[a]) Distance of the Cp centroid to the Zr-center.  [b]) Distance from axial Me group to the Zr-center.  [c]) Zr–H distance.  [d]) Zr–Me distance.  [e]) Zr–C distances are given.  [f]) Angles to $C_2H_4$ centroid.  [g]) For **7–10** R$^2$ replaced by R$^3$, for **11** and **12** $C_2H_4$, R$^2$ replaced by $CH_3$.

The computed geometrical parameters around the Zr-centers are mostly in good agreement with expected values from X-ray structure determinations of related complexes. The Zr–C bond distances from *Table 1* compare well with experimental values which cover a range of 2.257 to 2.346 Å for Zr–alkyl bonds [10a] [13a]. The Zr–Cp (centroid) separations were computed at remarkably constant values and the Zr–C$_2$H$_4$ distances increase with the coordination number (see *Table 1*). d$^0$ Zr-olefin X-ray data are not available, but one distance has been calculated by *ab initio* methods to be 2.45 Å [13b]. A d$^0$ Zr–allyl complex shows Zr–C separations between 2.375 and 2.525 Å [13c]. In general, the olefin ligand appears to be only weakly bound to the Zr-center. Steric interactions of the H(olefin)-atoms contribute to the position of the computed equilibrium bond lengths, which are especially significant for molecule **11**. In this context, it should be noted, that ethylene rotation about the Zr–C$_2$H$_4$ axis was in most cases found to be an energetic factor of minor importance, exhibiting activation barriers below 10 kcal/mol. In the case of **7**, it was required to introduce its rotamer **7′** with the olefin orientated perpendicular to its original position, because this also constituted a starting geometry in the theoretical analysis of the insertion reactions. The isomeric structure **7′** lies 2.4 kcal/mol above **7**.
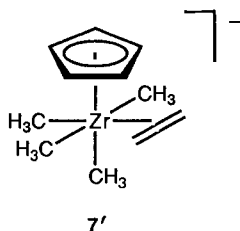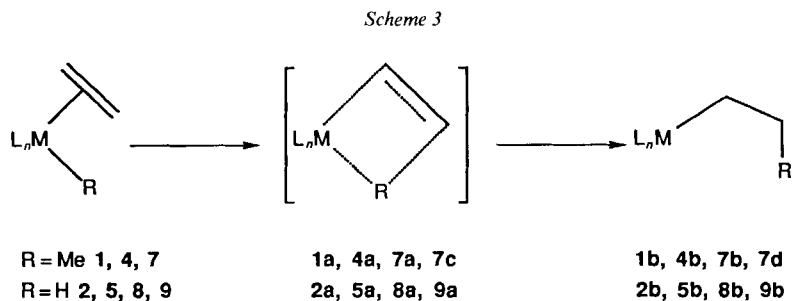


**7′**

*Table 1* also displays 'equatorial' angles of the optimized molecules **1–12**. These values expectedly reveal two major steric factors acting with varying influence in this plane of these molecules: Me groups tend to bend away from the olefin ligand and adjacent ligands to the Zr-bound H-atom are forming angles < 90° to it.

It turned out that the *cis-* $H/C_2H_4$ isomers **2, 5, 8, 9**, and **12** which are relevant for the insertion process are not in all cases the energetically preferred species. However, the energy difference between these species and their respective more stable isomers is generally so small that isomerism would not constitute any constraint for the energetic availability of any of the compounds **1–12** at room temperature.

*Potential-Energy Surfaces for Ethylene Insertion into* $Zr-CH_3$ *and* $Zr-H$ *Bonds.* To achieve some insight into the course of the eight possible Me or H migration reactions onto Zr-coordinated ethylene starting from **1, 2, 4, 5, 7**, and **7′, 8**, and **9**, MEHT optimizations were performed to yield either the corresponding Pr (**1b, 4b, 7b**, and **7d**) or Et (**2b, 5b, 8b**, and **9b**) compounds *via* the transition states **1a, 2a, 4a, 5a, 7a, 7c, 8a**, and **9a**, respectively (*Scheme 3*). Compound **7** allows for two principal reaction pathways to be taken depending on either $R^1$ or $R^2$ being the migrating Me moiety. As mentioned earlier, in case of $R^2$ migration onto the $C_2H_4$ ligand, the isomer **7′** is the more feasible starting system. The products of both elementary reactions thus differ in the final position of the Pr residue *cis* (**7b**) or *trans* (**7d**) to the Cp ring.

*Scheme 3*



R = Me **1, 4, 7**          **1a, 4a, 7a, 7c**          **1b, 4b, 7b, 7d**
R = H **2, 5, 8, 9**          **2a, 5a, 8a, 9a**          **2b, 5b, 8b, 9b**

$L_nZr = Me_4Zr^-, CpMe_2Zr, CpMe_3Zr^-$

The attempt to obtain an energy hypersurface of the Me or H migration starting from **11** or **12** failed because of a preferred ethylene dissociation during the insertion process. As mentioned earlier, the $C_2H_4$ ligand is especially in complex **11** only weakly bound to the Zr-center, and as migration of the one electron ligand $CH_3$ sets on further weakening occurs, which eventually provokes $C_2H_4$ elimination. A labilization of the olefinic moiety is also observed in case of H migration starting from **12**. Having not traced the exact electronic reason for these findings in **11** and **12**, it seems nevertheless obvious that olefin binding *trans* to the Cp ring of formally eight-coordinated complexes may easily be influenced by electronic changes in the ancillary ligand sphere. If our calculations match reality sufficiently well, it may be generalized that half-sandwich compounds of type **11** and **12** are not appropriate candidates for *Ziegler-Natta* catalysis.

Cuts through the multidimensional hypersurfaces of the other H or Me migration reactions were established by varying in either case of conversion two characteristic

parameters, namely the distance ($r$) of the migrating atom (C or H) to the C-atom C(2) of the coordinated ethylene ligand and the angle ($\alpha$) Zr–C(1)–C(2) at the Zr-ethylene moiety (see *Fig. 1*). In each point of the potential-energy surface, important geometrical degrees of freedom were optimized according to the parameters shown in *Table 2* and in *Table 8* of the *Appendix*. *Table 2* also contains relative energies and geometrical informations about prominent species on the hypersurfaces given in *Scheme 3*.
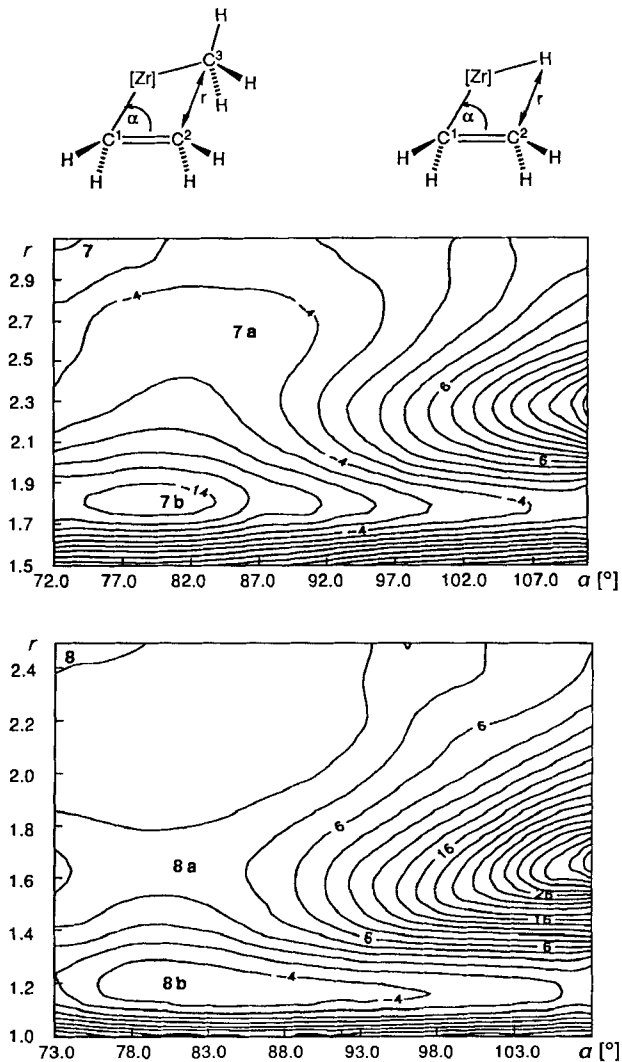


Fig. 1. *Cuts through the computed energy hypersurface for the ethylene insertion process into the Zr–CH₃ bond* ($7 \rightarrow 7b$) *and into a* $Zr-H$ *bond* ($8 \rightarrow 8b$). The plots were established by varying $\alpha$ and $r$ and optimizing the essential degrees of freedom around the Zr-center in each point of the surface. The values of the contour lines refer to kcal/mol.

Table 2. *Variation of Geometrical Parameters of the Energy Hypersurface of* Fig. 1 *and Those Represented by the Reaction Paths of* Fig. 2. Selected optimized values of the structures $1\rightarrow1b$, $2\rightarrow2b$, $4\rightarrow4b$, $7\rightarrow7d$, $8\rightarrow8b$, $9\rightarrow9b$. Not shown are values for the obtained parameters within the Zr fragments and the bond and torsion angles of the methylene protons.
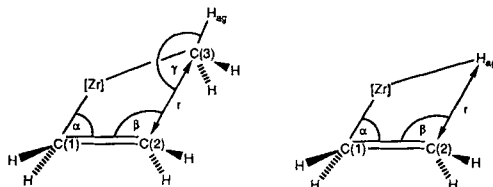


| | $E$ [kcal/mol]$^{a)}$ | $\alpha$ | $r$ | Zr—C(1) | C(1)—C(2) | Zr—H$_{ag}$ | $\beta$ | $\gamma$ |
|---|---|---|---|---|---|---|---|---|
| **1** | 22.2 | 73 | 3.18 | 2.56 | 1.49 | 2.95 | 116 | 173 |
| **1a** | 19.5 | 81 | 2.40 | 2.49 | 1.51 | 1.83 | 109 | 140 |
| **1b** | 0.0 | 75 | 1.73 | 1.90 | 1.84 | 1.82 | 111 | 127 |
| **2** | 19.7 | 72 | 2.44 | 2.45 | 1.48 | 1.58 | 110 | – |
| **2a** | 27.9 | 78 | 1.87 | 2.41 | 1.50 | 1.72 | 109 | – |
| **2b** | 0.0 | 81 | 1.17 | 2.03 | 1.76 | 2.03 | 107 | – |
| **4** | 23.0 | 74 | 2.77 | 2.62 | 1.50 | 2.89 | 118 | 166 |
| **4a** | 21.3 | 85 | 2.53 | 2.17 | 1.53 | 2.57 | 102 | 163 |
| **4b** | 0.0 | 84 | 1.77 | 2.05 | 1.75 | 1.83 | 115 | 109 |
| **5** | 17.3 | 73 | 2.48 | 2.55 | 1.48 | 1.62 | 106 | – |
| **5a** | 14.9 | 85 | 1.77 | 2.24 | 1.56 | 1.71 | 97 | – |
| **5b** | 0.0 | 78 | 1.19 | 2.04 | 1.78 | 1.98 | 106 | – |
| **7** | 14.5 | 73 | 2.80 | 2.67 | 1.50 | 2.84 | 118 | 155 |
| **7a** | 9.5 | 81 | 2.39 | 2.39 | 1.53 | 1.93 | 113 | 113 |
| **7b** | 0.0 | 79 | 1.83 | 2.08 | 1.81 | 1.83 | 122 | 122 |
| **7c** | 13.2 | 76 | 2.86 | 2.26 | 1.49 | 2.89 | 122 | 179 |
| **7d** | 24.3 | 86 | 2.23 | 2.26 | 1.61 | 1.90 | 114 | 120 |
| **7e** | 0.0 | 105 | 1.75 | 2.24 | 1.75 | 1.83 | 106 | 107 |
| **8** | 5.2 | 73 | 2.44 | 2.65 | 1.51 | 1.58 | 108 | – |
| **8a** | 8.0 | 79 | 1.57 | 2.40 | 1.64 | 1.73 | 102 | – |
| **8b** | 0.0 | 80 | 1.20 | 2.21 | 1.74 | 1.95 | 106 | – |
| **9** | 0.7 | 83 | 2.10 | 2.43 | 1.48 | 1.55 | 99 | – |
| **9a** | 3.4 | 79 | 1.52 | 2.27 | 1.58 | 1.68 | 104 | – |
| **9b** | 0.0 | 79 | 1.26 | 2.20 | 1.65 | 1.79 | 104 | – |

$^{a})$   Values relative to compound with lowest total energy, $\alpha$ = angle Zr—C(1)—C(2), $\beta$ = angle C(1)—C(2)—C(3), $\gamma$ = angle C(2)—C(3)—H$_{ag}$.

At this point it should be mentioned that modelling of organometallic reactivity by quantum-chemical methods always involves a simplified view when interpreting theoretically derived energetic data in terms of thermodynamic and kinetic parameters. The only justification for this type of approach is a good qualitative agreement with chemical plausibility and experimental results.

In *Fig. 1*, the computed energy hypersurfaces for the conversions $7 \rightarrow 7b$ and $8 \rightarrow 8b$ are shown as typical examples featuring the major characteristics of the other Me- or H-migration processes looked at as well. Choosing the presentation of only two of the obtained hypersurfaces seems justified by the general appearance of the computed energy

profiles for all these transformations ($1 \rightarrow 1b$, $2 \rightarrow 2b$, $4 \rightarrow 4b$, $5 \rightarrow 5b$, $7 \rightarrow 7d$, $9 \rightarrow 9b$) which are qualitatively similar for both H and Me migrations. Minor quantitative differences in the shape of the reaction profiles are, however, observed. Starting from **8**, the transformation is characterized by a slight increase in energy to reach the transition state **8a** followed by a steep downhill movement to reach the corresponding product **8b**. The surface of the Me migration starts out from **7** with a plateau-like flat area, which is somewhat inclined towards the product and ultimately joins into a steep energetic slope, before **7b** is reached. Thus, in contrast to the $8 \rightarrow 8b$ conversion, no distinct transition state is observed for the $7 \rightarrow 7b$ transformation. Nevertheless, a sectioning of the surface and the reaction path is suggested which is separating the initial plateau from the adjacent steep descent. At the junction of these two domains, we have defined the position of a pseudo-transition state **7a**, also for the cases of **1a**, **4a**, and **5a**. It should be mentioned at this point, that the optimization procedures for the compounds **1**, **4**, **5**, and **7** did not lead to **1b**, **4b**, **5b**, and **7b**, because the olefin ligand was allowed to adopt only restricted degrees of freedom as described in the *Appendix*.

As can be seen from *Table 2* and *Fig. 1*, the states **7a** and **8a** are reached by primarily opening the Zr–C(ethylene) angle ($\alpha$) and in case of Me migration some reorientation of the local Me group along the Zr–CH$_3$ axis. The geometrical distortions along the reaction path with respect to **7** and **8** lead to arrangements of an incipient carbenium-ion type [14] with a rather unsymmetrically coordinated olefin (see also orbital analysis to be discussed later). These findings are consistent with various theoretical investigations of such insertion processes carried out previously [15]. The activation barriers found in these studies on related systems are also low in the range of 4–12 kcal/mol [15].

The products **7b** and **8b** of the conversions calculated in this study contain a strong newly formed Zr–alkyl $\sigma$ bond and characteristically exhibit a relevant agostic C–H–Zr interaction. The latter is stronger for **7b** than for **8b**, as would be anticipated on the basis of the agostic ring sizes in these compounds. This behavior is symptomatic for Group-4b catalysts and was found by other investigations of possible reaction paths for *Ziegler-Natta* catalysis [16] as well.

The transformations $1 \rightarrow 1b$, $2 \rightarrow 2b$, $4 \rightarrow 4b$, $5 \rightarrow 5b$, $7 \rightarrow 7b$, $7' \rightarrow 7d$, $8 \rightarrow 8b$, and $9 \rightarrow 9b$ are sketched in *Fig. 2* depicting schematic energy profiles along their favored reaction courses.

Like the conversion $7 \rightarrow 7b$, almost all other reactions looked at during this study do not show a barrier of activation on going from an ethylene-Me complex to a Pr compound. An energetically flat initial profile is again followed by a steep decrease, which means that there is no pronounced transition state for the elementary steps $1 \rightarrow 1b$ and $4 \rightarrow 4b$. Once an ethylene molecule is attached to the Zr-center in these starting materials, migration of the Me group takes place spontaneously leading to the immediate formation of the Zr–Pr products.

In contrast to this behavior, migration of a H ligand in the processes $2 \rightarrow 2b$, and $8 \rightarrow 8b$ has to overcome a barrier (see *Fig. 2*). The calculated barriers are, however, *ca.* 2 and 3 kcal/mol, respectively. Well defined transition states (**2a** and **8a**, respectively) were found.

The Me-migration reaction $7' \rightarrow 7d$ gives rise to an exceptionally high barrier of *ca.* 11 kcal/mol with concomitant formation of a pronounced transition state **7c**. This difference compared to the other related processes is not too surprising, since the migration takes
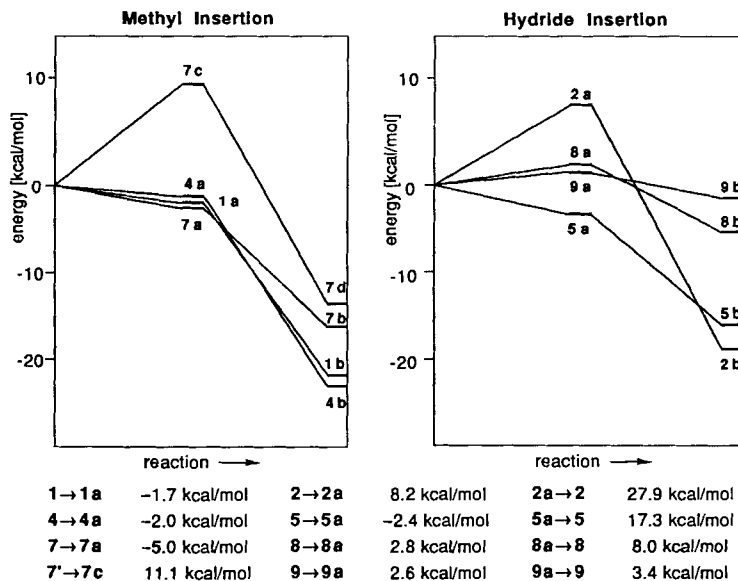
| 1 → 1a | -1.7 kcal/mol | 2 → 2a | 8.2 kcal/mol | 2a → 2 | 27.9 kcal/mol |
|---|---|---|---|---|---|
| 4 → 4a | -2.0 kcal/mol | 5 → 5a | -2.4 kcal/mol | 5a → 5 | 17.3 kcal/mol |
| 7 → 7a | -5.0 kcal/mol | 8 → 8a | 2.8 kcal/mol | 8a → 8 | 8.0 kcal/mol |
| 7' → 7c | 11.1 kcal/mol | 9 → 9a | 2.6 kcal/mol | 9a → 9 | 3.4 kcal/mol |

Fig. 2. *Schematic representation of the computed reaction paths for the transformations* 1 → 1b, 2 → 2b, 4 → 4b, 5 → 5b, 7 → 7b, 7c → 7e, 8 → 8b, *and* 9 → 9b. Optimized parameters see *Table 2*.

place in a chemically different migratory environment with different electronic prerequisites. As we will see later, this phenomenon can be understood on the basis of a characteristic $\pi$-donor effect exerted here by the Cp ligand. Therefore, the conversions 7' → 7d and the 9 → 9b must be viewed as special cases which should not be discussed in the same way as the 1 → 1b, 4 → 4b, and 7 → 7b reactions. With the energy values of *Fig. 2* at hand, it is tempting to try for a qualitative evaluation of the $k_p/k_t$ competing situation given in *Scheme 1*. For the interpretation of the $k_p/k_t$ ratio we have compared the deinsertion processes 2b → 2, 5b → 5, and 8b → 8 by mapping them on $k_t$ with the methyl migration steps 1 → 1b, 4 → 4b, and 7 → 7b representing $k_p$.

One can derive that the Me (and probably alkyl) migration processes are generally largely favored over the corresponding $\beta$-H elimination reactions. The corresponding rate constant $k_p$ should always be greater than $k_t$. This is in obvious agreement with the experimental data known from *Ziegler-Natta* catalysis at early-transition-metal centers [17].

Furthermore, it is important to note, that the 2b → 2, 5b → 5, and 8b → 8 conversions show only slightly decreasing barriers of activation with increasing coordination number. It is predicted that the $k_p/k_t$ ratio should not be oversensitive to this sort of chemical influence.

There is no direct experimental evidence to support this finding, but some plausibility may be given by the fact, that early-transition-metal *Lewis* acids quite often show varying numbers of *Lewis* bases to interact with them. Despite this observation, to our knowledge there is no report on *Ziegler-Natta* catalysis, which states a severe influence on the ratio of added co-ligands.

Despite their agostic stabilization the intermediates **1b**, **4b**, and **7b** are capable of subsequently taking up additional ethylene following the reaction path of the *Cossee* mechanism. Without going into details, it should be mentioned, that extensive geometrical optimizations were carried out to establish a hypersurface of these processes. Under these conditions, no kinetic barrier of the ethylene addition was found, and there was also no significant thermodynamic gain in energy for this reaction. This actually supports our assumption that olefin complexation influences $k_p$ only to a minor extent.

*Orbital Features of Ethylene-Insertion Reactions into* $Zr-CH_3$ *and* $Zr-H$ *Bonds.* The types of orbital conversions for the olefin insertion into transition-metal hydride and alkyl bonds [18] have been analyzed at various levels of sophistication of the calculational procedure and with different transition-metal centers using several coordination geometries. The investigations all have led to the conclusion that these reactions can geometrically and with regard to their orbital analysis be divided into two stages: a slippage of the olefin ligand taking place first with formation of an 'incipient carbenium ion' structure [14b], followed by a subsequent orientation of the migrating group towards the C-atom C(2) of the olefinic system. The same overall features of the general orbital situation were found for all conversions discussed in this paper (**1** → **1b**, **2** → **2b**, **4** → **4b**, **5** → **5b**, **7** → **7b**, **7′** → **7d**, **8** → **8b**, **9** → **9b**), regardless whether Me or H was the migrating group and independent of the coordination number of the starting compound.

It was noted earlier that our investigation in part did not reveal energetically defined transition states for the Me-insertion reactions. However, it became obvious that the reaction paths in these cases allowed a sectioning of certain orbital characteristics. We have introduced prominent geometries (hitherto called transition states) **1a**, **4a**, and **7a** which in each case account for the transition between the described two motional steps and concomitantly sections of unique orbital features. *Tables 3* and *4* list the total overlap populations for the broken and formed bonds for all conversions under consideration.

For the ethylene-Me or hydrido-Zr starting compounds, it is remarkable that the Zr–C(ethylene) bonds show a relatively small electronic population in all coordination geometries. This means that the olefin is only loosely attached to the Zr-center with the

Table 3. *Changes in Overlap Population of Crucial Bonds during Ethylene Insertion into a* $Zr-CH_3$ *Bond.* Transformations 1→1b, 4→4b, 7→7b, and 7→7d.

|      | Zr–C(1) | Zr–C(2) | C(2)–C(3) | Zr–C(3) | Zr–H$_{ag}$ |
|------|---------|---------|-----------|---------|-------------|
| **1**  | 0.0580 | 0.0133  | −0.0041   | 0.4029  | −0.0591 |
| **1a** | 0.1123 | −0.0119 | −0.0001   | 0.3566  | 0.0472  |
| **1b** | 0.5893 | 0.0194  | 0.6245    | −0.0709 | 0.0837  |
| **4**  | 0.0281 | 0.0406  | −0.0016   | 0.3535  | −0.0542 |
| **4a** | 0.2091 | −0.0361 | 0.0391    | 0.3231  | −0.0472 |
| **4b** | 0.5402 | −0.0266 | 0.6121    | −0.0558 | 0.0914  |
| **7**  | 0.0396 | 0.0266  | 0.0000    | 0.2926  | −0.0555 |
| **7a** | 0.1487 | −0.0611 | 0.1062    | 0.2229  | −0.0429 |
| **7b** | 0.4724 | 0.0126  | 0.5379    | −0.0422 | 0.0909  |
| **7c** | 0.0289 | 0.0313  | −0.0049   | 0.3746  | −0.0599 |
| **7d** | 0.2563 | −0.0016 | 0.2390    | 0.0857  | 0.0496  |
| **7e** | 0.4013 | −0.0921 | 0.6142    | −0.0464 | 0.1011  |

Table 4. *Development of Overlap Populations of Bond Changes Involved in Ethylene Insertion into a Zr—H Bond. Transformations* 2→2b, 5→5b, 8→8b, *and* 9→9b.

|     | Zr—C(1) | Zr—C(1) | C(2)—H | Zr—H |
|-----|---------|---------|--------|------|
| **2**  | 0.0252 | 0.0228  | 0.0021 | 0.7009 |
| **2a** | 0.0964 | −0.0479 | 0.0902 | 0.5771 |
| **2b** | 0.5205 | −0.0810 | 0.6402 | 0.0277 |
| **5**  | 0.0192 | 0.0331  | 0.0041 | 0.6831 |
| **5a** | 0.1988 | −0.0449 | 0.1269 | 0.5729 |
| **5b** | 0.5099 | −0.0604 | 0.7042 | 0.0762 |
| **8**  | 0.0175 | 0.0394  | 0.0000 | 0.6967 |
| **8a** | 0.2108 | −0.0263 | 0.2927 | 0.4103 |
| **8b** | 0.3905 | −0.0816 | 0.7051 | 0.0693 |
| **9**  | 0.0629 | 0.0321  | 0.0030 | 0.6745 |
| **9a** | 0.2026 | −0.0677 | 0.3185 | 0.4113 |
| **9b** | 0.2933 | −0.1060 | 0.6009 | 0.1795 |

consequence of forming a strong C(2)—C(3) or C—H, and a strong M—C(1) bond in the insertion products naturally expressed in the corresponding orbital situations. In comparison to this, a general increase in bonding of the 'terminal' C-atom (C(1)) to the metal center is found for the transition states while the 'internal' C-atom (C(2)) even becomes orbitally repelled by the metal center (see populations of the corresponding bonds, *Tables 3* and *4*). This latter observation is well in accord with the idea of an 'incipient carbenium ion' type structure, where the carbenium character is localized at C(2) of the Zr-bound ethylene ligand. This interpretation is further stressed by the finding of large orbital coefficients at these C-atoms in the LUMOs of all transition states looked at.

From *Table 3*, it can be seen that the six- and seven-coordinated species **1a** and **4a** show almost no contact between the ethylene ligand and the Me group, whereas in the case of eight-coordination considerable contact is already found because of a closer distance of the relevant atoms. Apparently this is caused by an enhanced steric crowding in this latter case. In contrast, the Zr—CH$_3$ or Zr—H bond populations generally seem to decline for all transition states in all transformations on going from lower to higher coordination numbers.

The Zr—ethyl or Zr—propyl compounds **1b**, **2b**, **4b**, **5b**, **7b**, **7d**, **8b**, and **9b** as products of the migration step are characterized in almost all cases by a fully installed Zr—alkyl bond and are, as denoted earlier, stabilized by relatively strong Zr—H—C agostic interactions. This is again expressed by the orbital populations of the corresponding bonds (see *Tables 3* and *4*).

Although *Table 3* and partly *Table 4* implicate overall weaker Zr—C and Zr—H bonds with increasing coordination numbers, this is not reflected in differences of comparable bond populations of all prominent molecular states on the reaction paths (see *Fig. 2*). This is the reason why the computed activation energies of the insertion processes leading to **1b**, **2b**, **4b**, **5b**, **7b**, **8b**, and **9b**, respectively, do not show a great dependency on the coordination number.
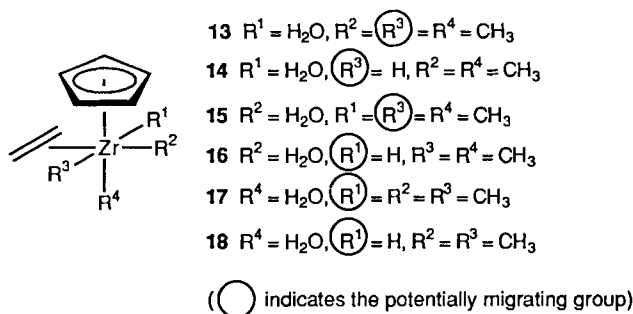
*Orbital Influence of π-Donor Ligands on the Me- and H-Migration Reactions.* The *Ziegler-Natta* polymerization is quite often conducted under circumstances which involve O-containing ligand components. The O-functionalities may originate from solvents, ligands in the catalyst precursors or added co-catalysts [6b] [19]. It seems to be

likely that the highly *Lewis*-acidic *Ziegler-Natta* metal center seeks interaction with any provided O-donor function during a catalytic process. Although a large amount of empirical data has been accumulated on the effects of different types of donors on this catalysis, the underlying mechanistic influence is not very well understood. This is mainly due to the difficulty to specifically identify the actual catalytically active species. Therefore, it was tempting to probe theoretically the influence of O-ligands on the ethylene insertion into $Zr-CH_3$ and $Zr-H$ bonds.

Normally, O-functionalities are of a single faced or conical $\pi$-donor category. Relating to known and structurally well characterized eight-coordinated half-sandwich complexes of the type $[Zr(Cp)Cl_3L_2]$ ($L = \pi$-donor, among others $L = H_2O$), we have constructed hypothetical molecules **13** and **14** with the theoretically feasible $\pi$-donor $H_2O$ as starting compounds for an exploratory treatment of the respective Me and H migration processes on Zr-bound ethylene. First, we checked whether **13** and **14** which provide a 'ready-to-insertion structure' exhibiting the olefin and migrating group in *cis*-orientation would be the energetically favored geometrical isomers. Surprisingly, an extensive optimization procedure has revealed that **13** represents an energy minimum with respect to all possible isomers, and that **14** was energetically quite close to it. It should be mentioned that a $H_2O$ ligand would for obvious reasons not be a good ligand candidate for *Ziegler-Natta* polymerizations. It is, however, perfectly suited to mimic the necessary electronic features of an O-containing ancilliary ligand. The $H_2O$ molecule represents a single faced $\pi$-donor which in our analysis is bound to the Zr-center in a 'planar' mode (Zr, O, and both H's in one plane). This binding feature of $\pi$-donors is found quite often in *Lewis*-acidic $d^0$-transition-metal chemistry [11a] [20]. The $H_2O$ ligand in compounds **13** and **14** could principally give rise to rotamers. We have defined the angle between the $H_2O$ plane and the plane of migration as $\varphi$ (see *Table 5*). Thus, the prominent orientations $\varphi = 90°$ and $\varphi = 0°$ denote that the $\pi$-donor orbital is lying in the plane of migration or perpendicular to it, respectively.

*Fig.3* shows the potential-energy hypersurfaces for the Me and H migration to ethylene starting from **13** and **14** leading to the propyl (**13b**) and ethyl (**14b**) products *via* the transition states **13a** and **14a**, respectively. The energy surfaces were established in the same manner as those in *Fig. 1*.

In contrast to the related migration process **7** → **7b**, we find a remarkable difference in the reaction profile for the **13** → **13b** transformations. A distinct transition state appears which is separated from **13** by *ca.* 12 kcal/mol. Since the energetic differences between **7**
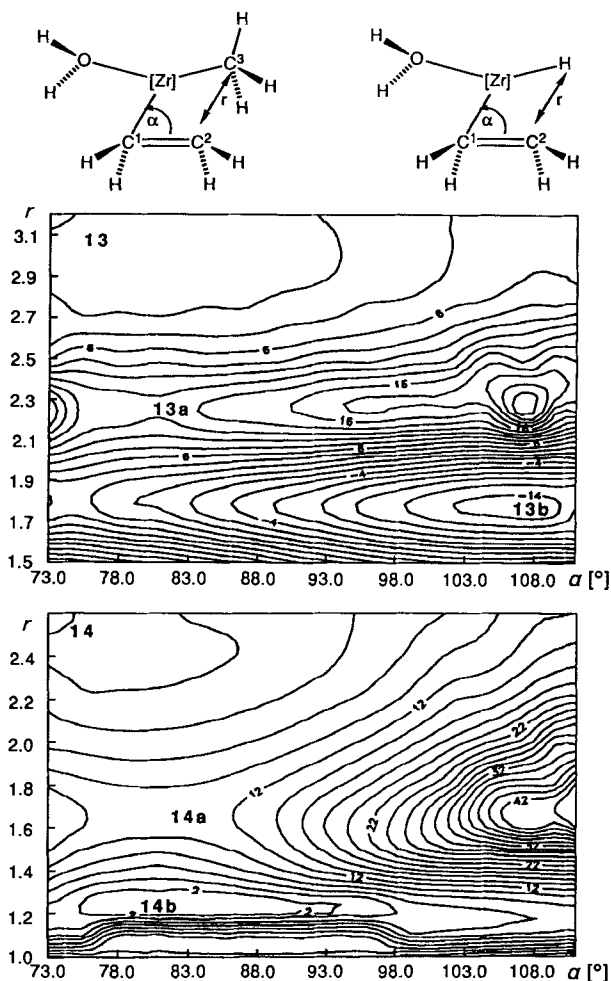


**13** $R^1 = H_2O$, $R^2 = \textcircled{R^3} = R^4 = CH_3$

**14** $R^1 = H_2O$, $\textcircled{R^3} = H$, $R^2 = R^4 = CH_3$

**15** $R^2 = H_2O$, $R^1 = \textcircled{R^3} = R^4 = CH_3$

**16** $R^2 = H_2O$, $\textcircled{R^1} = H$, $R^3 = R^4 = CH_3$

**17** $R^4 = H_2O$, $\textcircled{R^1} = R^2 = R^3 = CH_3$

**18** $R^4 = H_2O$, $\textcircled{R^1} = H$, $R^2 = R^3 = CH_3$

($\bigcirc$ indicates the potentially migrating group)

Fig. 3. *Computed energy-surface plot for the ethylene insertion process into the* $Zr-CH_3$ *bond* (**13** → **13b**) *and into a* $Zr-H$ *bond* (**14** → **14b**). The plots were established by varying $\alpha$ and $r$ and optimizing the essential degrees of freedom around the Zr-center in each point of the surface. The values of the contour lines refer to kcal/mol.

and **7b**, and **13** and **13b** are approximately the same (14.5 and 15.1 kcal/mol, respectively), it must be concluded that the transition state **13a** suffers from a severe destabilization caused by the introduction of the $H_2O$ $\pi$-donor ligand.

When **13a** is approached, the $H_2O$ ligand is forced to rotate its plane from the optimized value $\varphi = 87°$ (**13**) with respect to the migration plane to $\varphi = 44°$ and turning back to $\varphi = 90°$ in **13b**. Apparently, this effect is caused by superimposition of a repulsive electronic force in **13a** whose origin will be traced in the later context. The insertion of ethylene into a Zr–H bond, *i.e.* the conversion of the $\pi$-donor substituted molecules **14** → **14a** → **14b**, has to face a geometrically similar but energetically much less pronounced transition state situation as in **13** → **13a** → **13b** (see *Table 5*). Almost no energetic

Table 5. *Variation of Geometrical Parameters of the Energy Hypersurface of* Fig. 4. Selected optimized values of the structures **13→13b, 14→14b, 15→15b, 16→16b, 17→17b, 18→18b**. Not shown are values for the obtained parameters within the Zr fragments and the bond and torsion angles of the CH$_2$ protons.
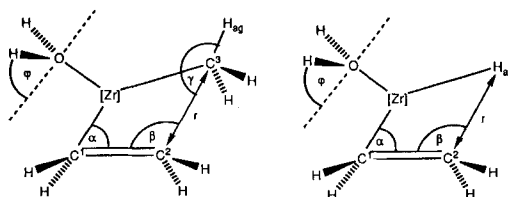


| | $E$ [kcal/mol][a]) | $\alpha$ | $r$ | Zr–C(1) | C(1)–C(2) | Zr–H$_{ag}$ | $\beta$ | $\varphi$ |
|---|---|---|---|---|---|---|---|---|
| **13** | 15.1 | 73 | 3.12 | 2.70 | 1.50 | 2.85 | 118 | 87 |
| **13a** | 27.3 | 81 | 2.27 | 2.32 | 1.58 | 2.33 | 116 | 44 |
| **13b** | 0.0 | 108 | 1.75 | 2.26 | 1.74 | 1.94 | 106 | 89 |
| **14** | – 0.2 | 73 | 2.40 | 2.53 | 1.50 | 1.58 | 100 | 90 |
| **14a** | 11.6 | 80 | 1.67 | 2.34 | 1.57 | 1.67 | 101 | 88 |
| **14b** | 0.0 | 81 | 1.2 | 2.18 | 1.74 | 2.00 | 105 | 90 |
| **15** | 12.1 | 73 | 2.73 | 2.89 | 1.45 | 2.69 | 125 | 81 |
| **15a** | 16.5 | 87 | 2.25 | 2.25 | 1.57 | 2.36 | 112 | 61 |
| **15b** | 0.0 | 101 | 1.73 | 2.16 | 1.77 | 1.99 | 112 | 80 |
| **16** | 2.3 | 83 | 2.21 | 2.64 | 1.51 | 1.59 | 100 | 90 |
| **16a** | 6.9 | 79 | 1.66 | 2.40 | 1.57 | 1.67 | 102 | 88 |
| **16b** | 0.0 | 79 | 1.23 | 2.23 | 1.72 | 1.91 | 105 | 84 |
| **17** | 11.3 | 73 | 2.97 | 2.49 | 1.45 | 2.86 | 120 | 71 |
| **17a** | 11.6 | 88 | 2.38 | 2.34 | 1.56 | 2.32 | 110 | 50 |
| **17b** | 0.0 | 83 | 1.75 | 2.16 | 1.74 | 1.88 | 122 | 41 |
| **18** | 9.4 | 74 | 2.08 | 2.69 | 1.50 | 1.58 | 110 | 60 |
| **18a** | 12.0 | 80 | 1.67 | 2.54 | 1.52 | 1.69 | 103 | 59 |
| **18b** | 0.0 | 102 | 1.16 | 2.21 | 1.76 | 2.02 | 108 | 51 |

[a])  Energy values relative to positional isomer with lowest total energy, $\alpha$ = angle Zr–C(1)–C(2), $\beta$ = angle C(1)–C(2)–C(3) or C(1)–C(2)–H, $\varphi$ = torsion angle H–O–Zr–Cp centroid.

difference between **14** and **14b** (0.2 kcal/mol) is observed which, in comparison to that between **8** and **8b** (−5.2 kcal/mol), has not charged drastically, but is greater than in the analogous **7/7b** and **13/13b** case. The reduced repulsive $\pi$-influence of H$_2$O in **14a** is also expressed by practically unchanged values of $\varphi$ on going along **14 → 14a → 14b**.

In further investigations on the Me and H migration reactions, the effect of the geometric position of the H$_2$O $\pi$-donor ligand relative to the olefin has been tested by calculating fully optimized two dimensional energy hypersurfaces for the insertions starting from **15–18**. This was carried out in the same way as had been done for the processes **13 → 13b** and **14 → 14b**. *Table 5* summarizes relative energy values and selected geometrical parameters of prominent species (starting materials **15–18**, transition states **15a–18a**, and products **15b–18b**) of the computed reaction paths. For the **15 → 15b** and **16 → 16b** conversions, we have found similar general energetic features as for the **13 → 13b** and **14 → 14b** transformations, *i.e.* the reaction paths get destabilized in the region of the transition states albeit to a lesser extent. This obviously means that the $\pi$-donor influence on these migration processes is diminished under these circumstances.

Taking the *Cossee* mechanism according to *Scheme 1*, and assuming that only one $\pi$-donor might be present in the migratory plane of compounds with coordination number 6–8, we postulate a $\pi$-donor-modified *Cossee* reaction of *Scheme 4*. From the foregoing analyses, we can state that $k_p(1) > k_p(2)$. Due to the positional flip of the alkyl chain, these should be an alternating influence of the $\pi$-donation. However, the polymerization would be rate-determined by $k_p(2)$. In catalysis, a $\pi$-donor would always exert its maximum influence on $k_p$, regardless of its original position in the plane of migration of the catalyst molecule.

*Scheme 4*



[C] = growing alkyl chain;
$D(\pi) = \pi$-donor ligand
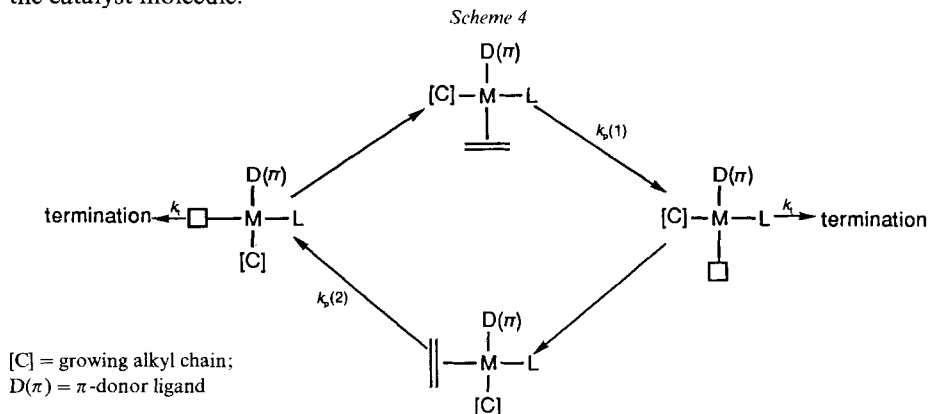
The $\pi$-donor in a position perpendicular to the plane of migration ($7 \rightarrow 7b$, $8 \rightarrow 8b$ compared to $17 \rightarrow 17b$, $18 \rightarrow 18b$, respectively) does in first approximation not show any energetic influence on the insertion processes under consideration. This result emphasizes on the fact that substituent effects appear most prominently in migratory transformations in the plane of migration, a circumstance which has also been realized in an earlier theoretical investigation of the CO insertion reaction [21]. It should be noted that, although we have confined our discussion to the cases of eight-coordinated complexes, we have thoroughly theoretically investigated all the other possibilities of migration processes within seven- and six-coordination. It was found that the energetics of these transformations show the same substitutional trends as in eight-coordination. That means that the $\pi$-donor shows analogous effects in ethylene insertions regardless of the considered coordination number in the starting complexes. It was also tested what influence two $H_2O$ $\pi$-donors arranged in the plane of migration of the Me insertion reaction would have. It turned out that two donors cause a higher activation barrier than just one, but the influence caused by two substituents was less than additive.

Irrespective of the starting component **14**, **16**, and **18**, or **13**, **15**, and **17** when comparing the $\pi$-donor influence on H and Me migrations, one finds as already indicated for **14** compared to **13** a markedly smaller influence on the H transfer to Zr-bound ethylene, *i.e.* destabilization of **14a**, **16a**, and **18a** (see *Table 5*).

In addition, considering the energetic differences of the hydride deinsertion processes (**14a** $\rightarrow$ **14b**, **16a** $\rightarrow$ **16b**, **18a** $\rightarrow$ **18b**) which stand for the major contribution to $k_t$, they appear only marginally be influenced by the $H_2O$ donor, since both transition states and products are obviously destabilized to almost the same (but also relatively small) extent.

While the $\pi$-donor influence on **14a**, **16a**, and **18a** has the same orbital origin as for **13a**, **15a**, and **17a**, the destabilization of **14b**, **16b**, and **18b** could not be clearly be attributed to a specific orbital effect. Thus, even if the destabilization of **14b**, **16b**, and **18b** would be due to an artefact of the calculations, the effect of a lowered $\pi$-donor influence on the transition states of hydride migrations would remain. This differentiation concerning the type of migration process, *i.e.* great retardation of the alkyl migration, small deceleration of the hydride migration, may be important for the design of olefin oligomerization catalysts, since it would provide a chemical handle to eventually control the $k_p/k_t$ ratio *via* an appropriate adjustment of the $\pi$-donor substitution patterns.

To further verify the relevance of the $\pi$-donor variation in these processes, we have computatively modified the $H_2O$ molecule in the transformations $13 \to 13b$, $14 \to 14b$, $15 \to 15b$, $16 \to 16b$, $17 \to 17b$, and $18 \to 18b$ by artificially varying the electronegativity of the O-atom, thus simulating *e.g.* F-, N-, or C-containing $\pi$-donor ligands. The results are comprised in *Table 6*.

Table 6. *Artificial Donor Variation on Conversion* $13 \to 13b$, $14 \to 14b$, $15 \to 15b$, $16 \to 16b$, $17 \to 17b$, *and* $18 \to 18b$. Energy values [kcal/mol] relative to compound with lowest optimization energy.

| | Starting compound | Transition state | Product |
|---|---|---|---|
| $\pi$-Donor emulating F | | | |
| $13' \to 13a' \to 13b'$ | 13.09 | 18.50 | 0 |
| $14' \to 14a' \to 14b'$ | 3.20 | 10.90 | 0 |
| $15' \to 15a' \to 15b'$ | 14.73 | 15.67 | 0 |
| $16' \to 16a' \to 16b'$ | 4.49 | 8.96 | 0 |
| $17' \to 17a' \to 17b'$ | 36.70 | 12.8 | 0 |
| $18' \to 18a' \to 18b'$ | 13.87 | 14.30 | 0 |
| $\pi$-Donor emulating N | | | |
| $13' \to 13a' \to 13b'$ | 18.97 | 52.77 | 0 |
| $14' \to 14a' \to 14b'$ | 4.61 | 11.11 | 0 |
| $15' \to 15a' \to 15b'$ | 10.53 | 20.42 | 0 |
| $16' \to 16a' \to 16b'$ | 9.22 | 9.77 | 0 |
| $17' \to 17a' \to 17b'$ | 37.68 | 25.42 | 0 |
| $18' \to 18a' \to 18b'$ | 13.70 | 14.76 | 0 |
| $\pi$-Donor emulating C | | | |
| $13' \to 13a' \to 13b'$ | 22.36 | 62.20 | 0 |
| $14' \to 14a' \to 14b'$ | 5.18 | 10.84 | 0 |
| $15' \to 15a' \to 15b'$ | 7.57 | 25.56 | 0 |
| $16' \to 16a' \to 16b'$ | 6.08 | 13.66 | 0 |
| $17' \to 17a' \to 17b'$ | 3.30 | 11.43 | 0 |
| $18' \to 18a' \to 18b'$ | 12.99 | 14.85 | 0 |

As anticipated, the data of *Table 6* reveal a drastic increase of the activation barriers for the Me migration varying from 5 kcal/mol (F) to 40 kcal/mol (C). In contrast, as expected from the foregoing analysis, the H-migration reaction (**14 → 14b**) seems to be almost insensitive to such a substitutional change. Thus, the $k_p/k_t$ ratio of a *Ziegler-Natta* catalysis should be quite dependent on the type of $\pi$-donor in the ancillary ligand sphere. Since the nature of a $\pi$-donor ligand can easily be adjusted in catalytic experiments, *e.g.* by the addition of suitable co-ligands, this theoretical finding may be taken as a challenge for systematic investigations on the tuning of *Ziegler-Natta* catalysis.

It has been proposed in the literature [22] that, in Group-IVb *Ziegler-Natta* chemistry, there should be an enhancement of the overall polymerization yields with increasing donating abilities of added co-ligands. Since there is not necessarily a dependency of the polymerization rate $k_p$ on this yield, and since no distinction of $\sigma$- and $\pi$-donor abilities of the co-ligands was made, we think that these proposals are not contradictive to our theoretical analysis.

On the contrary, several other groups [6b] [20] have found that the addition of $\pi$-donor ligands to *Ziegler-Natta* catalysts leads to oligomerization products, potentially *via* adjustment of the $k_p/k_t$ ratio with the same trends as resulting from our theoretical analysis: the presence of energetically high lying $\pi$-donors gives rise to C,C-coupling products of lower molecular weight.

Tracing the orbital basis of the observed pronounced $\pi$-donor effect, we found a dominating orbital interaction in the MO correlation diagrams of the exemplary $13 \rightarrow 13a \rightarrow 13b$ conversion which accounts for most of the activation barrier. For enhancement of the relevant orbital interactions, the reaction $13' \rightarrow 13a' \rightarrow 13b'$ analogous to $13 \rightarrow 13a \rightarrow 13b$ was chosen but with replacement of $H_2O$ by $CH_2^{2-}$ and with fixation of the $\pi$-donor orbital parallel to the plane of migration. The dominating orbital conversion which represents the transformation of the HOMOs now is especially suited for a representation in contour plots (see *Fig. 4*).
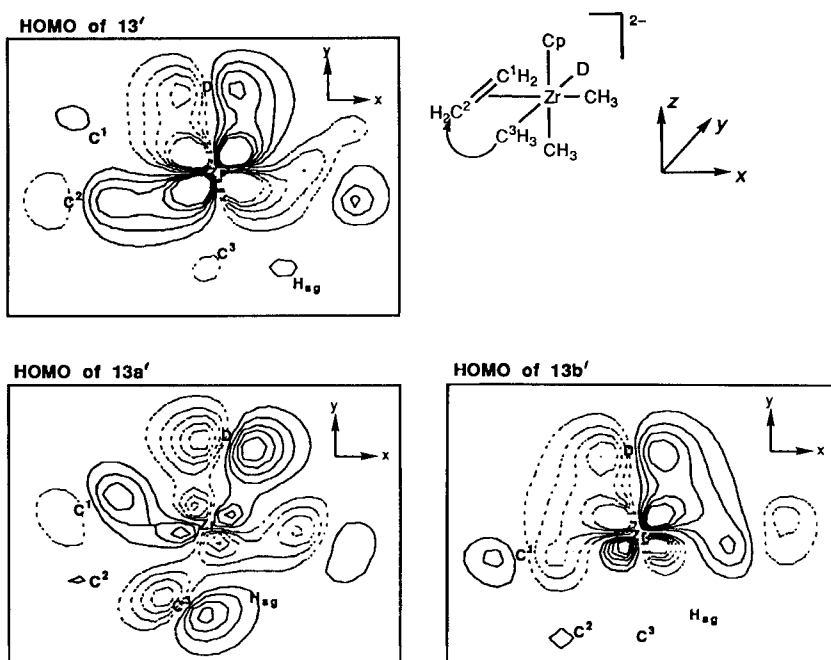


Fig. 4. *Contour plots of $\psi$ of the dominating orbital transformation of $13' \rightarrow 13a' \rightarrow 13b'$ (HOMO) sketched along the computed reaction path of $13 \rightarrow 13b$* (contour lines: ±0.1, ±0.08, ±0.06, ±0.04, ±0.02). D denotes the position of the $\pi$-donor C-atom and $H_{ag}$ the position of the agostic H-atom. $C^3$ corresponds to the $CH_3$ group and $C^1$ and $C^2$ to the olefinic C-atoms.

The HOMO transformation of the $13' \rightarrow 13a' \rightarrow 13b'$ transition is for $13'$ and $13b'$ characterized by a strong and binding $\pi$-donor interaction with mainly $d_{xy}$ character in the plane of migration. In $13'$ and $13a'$, the HOMO also reveals a strong binding interaction with the ethylene $\pi^*$ function. In $13'$ (Fig. 4), there is no interaction with any orbital of the migrating group, since especially its $\sigma$-type lobe ($\sigma(CH_3)$) is located in the nodal plane of the $d_{xy}$ orbital. The transition state $13a'$ in the HOMO exhibits a non-bonding situation of the olefin $\pi$ and $\pi^*$ orbitals and the $\sigma(CH_3)$ typical of the Zr-mediated ethylene/Me approach. Furthermore, the $13a'$ HOMO suffers from an additional antibonding contribution between the ethylene/Me moiety and the $d_{xy}$ metal orbital character. The latter effect may be viewed as an expression of bumping of filled orbital character during the migration process. Apparently, the Me group migrates as a methyl anion, whose $\sigma$ electrons start to delocalize over the $C_1$–$C_3$ moiety in $13a'$ as the Me/ethylene contact is turned on. A non-satisfactory geometrical situation of the $C_1$–$C_3$ unit causes interaction with the $d_{xy}$ orbital. Since $d_{xy}$ character due to the $\pi$-donor interaction is partly inherent in filled orbitals – mainly in the HOMO – four-electron-repulsive terms result.

These repulsive contributions are to a certain extent diminished by mixing a significant deal of $\pi$-donor/$d_{xy}$ antibonding function into the HOMO, thereby giving rise to an electronic situation which comes close to a nonbonding interaction between the $\pi$-donor orbital, functions of the $C_1$–$C_3$ moiety and the $d_{xy}$ orbital. The mixing occurs such that the metal character decreases in the HOMO as can clearly be seen from Fig. 4. As a consequence, the $\pi$-donor in $13a'$ as well as in $13a$ is no longer strongly bound to the metal. Rotation about the Zr-D($\pi$) axis gets easier. The reason why the rotation in $13a$ is then actually observed is given by the tendency for reducing the $\pi$-donor's out-of-phase secondary-type interaction with the growing p-orbital lobe at $C_3$ (Fig. 4). It is an inter-ligand orbital contact of two cis-positioned groups, which gives rise to extra repulsion. For the migration process $15 \rightarrow 15a \rightarrow 15b$ where the $\pi$-donor is located trans to the ethylene group, this effect is not anticipated.

In the HOMO of $13b'$ the $d_{xy}$ orbital content and the bonding $\pi$-donor interaction is restored again to a great extent. Only marginal orbital bumping of the same type as in $13a'$ with the $\sigma$(propyl) and the $\sigma(CH_3)$ lobes occurs. For geometric reasons, the Pr and the Me group are not completely located in the nodal plane of $d_{xy}$.

Despite the general situation of a $d^0$ system, we are dealing in these complexes with occupied $d_{xy}$-character orbitals originating primarily from the interaction with the $\pi$-donor ligand. For $1a$, $4a$, and $7a$, there is no energetic destabilization of the transition states, because without the $\pi$-donor interaction the $d_{xy}$ orbital character is majorly available from unoccupied functions in the LUMO region. Thus, four-electron repulsive interactions with the forming Pr moiety and $d_{xy}$ character do not appear.

Finally, it should be mentioned that the calculated relatively high energetic barrier for the $7' \rightarrow 7c \rightarrow 7d$ conversion (see Table 2) can be explained in the same manner as for $13 \rightarrow 13a \rightarrow 13b$ or $13' \rightarrow 13a' \rightarrow 13b'$, since the Cp ligand represents a $\pi$-donor ligand, with the possibility of $\pi$-interaction in the plane of migration.

As mentioned earlier, the H migration of $14 \rightarrow 14a \rightarrow 14b$ does not show an overall energetical situation distinguished much from that of the transformation $8 \rightarrow 8b \rightarrow 8c$, and consequently almost no transition state destabilization comparable to that of the $13 \rightarrow 13a \rightarrow 13b$ transition is observed. When H is the migrating group excessive anti-

bonding contacts with filled Zr d orbital character can for geometric, *i.e.* overlapping, reasons obviously be avoided.

**Conclusions.** – Me or H migrations in formally six-, seven-, or eight-coordinated Zr complexes have been shown to be almost independent on the coordination number of the starting components (*Scheme 5*). In accordance with other theoretical analyses [15] [18] and with experimental results [3] [17], they do not exhibit large activation barriers.

*Scheme 5*



$L_nZr = Me_4Zr^-, CpMe_2Zr, CpMe_3Zr^-$
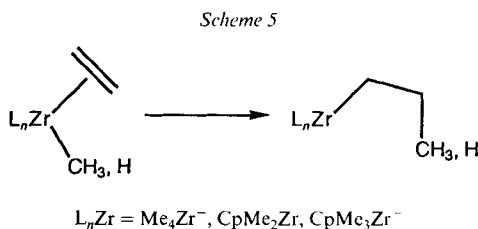
The products of these migrational processes are significantly stabilized by an agostic interaction, which is, however, not strong enough to suppress the addition of another olefin monomer to carry on with the catalytic polymerization process.

In addition, it was analyzed, that the Me migration can be retarded by the introduction of $\pi$-donor ligands in the plane of migration. A destabilizing electronic effect on the transition state for these conversions, qualitatively independent of the coordination number, has been identified. This $\pi$-donor effect is dependent of the electronegativity of the $\pi$-donor ligand and increases with lower electronegativity of the central atom of this group. The related migration of H- to Zr-bound ethylene shows a parallel trend in energetic dependence, but to a much lesser extent. The reverse process, the $\beta$-H elimination, which is the main concurrence reaction in *Ziegler-Natta* catalysis is not influenced by variation of the $\pi$-donor abilities of the ligand sphere. This suggests that in actual *Ziegler-Natta* catalysis the chain length determining ratio $k_p/k_t$ may be adjusted by the chemical influence of appropriate co-ligands with $\pi$-donor properties.
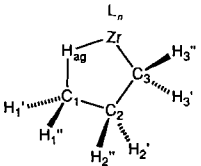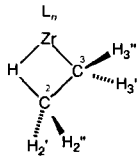
**Appendix to the Calculations.** – The parameters used in MEHT calculation [12] are given in *Table 7*. They were taken from earlier work [23].

Table 7. *Extended* Hückel *Parameters Used in the MEHT Calculations*

| Element | Orbital | $H_{ii}$ [eV] | $\zeta_1$ | $\zeta_2$ | $C^1$ | $C^2$ | Ref. |
|---------|---------|-----------|-----------|-----------|-------|-------|------|
| H | 1s | −13.6 | 1.30 | | | | [23a] |
| C | 2s | −21.4 | 1.625 | | | | [23a] |
| | 2p | −11.4 | 1.625 | | | | |
| N | 2s | −26.0 | 1.95 | | | | [23a] |
| | 2p | −13.4 | 1.95 | | | | |
| O | 2s | −32.3 | 2.275 | | | | [23a] |
| | 2p | −14.8 | 2.275 | | | | |
| F | 2s | −40.00 | 2.425 | | | | [23a] |
| | 2p | −18.10 | 2.425 | | | | |
| Zr | 4d | −12.1 | 3.835 | 1.505 | 0.6211 | 0.5796 | [23b] |
| | 5s | −10.1 | 1.776 | | | | |
| | 5p | − 6.86 | 1.817 | | | | |

To reduce the amount of computational work, complexes 1–2 were structurally optimized applying some restrictions in the search on the energy hypersurfaces according the following iterative procedures: starting from an idealized coordination geometry all metal-to-ligand bond distances were optimized joined by a variation of all independent bond and dihedral angles around the Zr-center to find the minimum energy arrangement. This procedure was then repeated twice or three times. In all stages of these processes, the olefin ligand was kept symmetrically bound, so that any sort of hinging or slippage motions representing prestages of migrational processes were not allowed. All Me groups had a fixed pseudotetrahedral geometry with a C–H bond distance of 1.12 Å, which was also used for $CH_2$ groups. The choice of structural parameters within and connecting to atoms in the plane of migration varied in the establishment of the hypersurfaces for H or Me migration is listed in Table 8.

Table 8. *Survey of Optimized 'In Plane' Degrees of Freedom in Me and H Migrations*



| Me Migration | Both | H Migration |
|---|---|---|

| | Angles | |
|---|---|---|
| $C_3C_2C_1$ | $ZrC_3C_2^a)$ | $C_3C_2H$ |
| $C_2C_1H_{ag}$ | $H_3'C_3H_3''$ | |
| $C_2C_1H_1'$ | $C_2C_3H_3'$ | |
| $C_2C_1H_1''$ | $C_2C_3H_3''$ | |
| $H_1'C_1H_1''$ | $C_3C_2H_2'$ | |
| | $C_3C_2H_2''$ | |
| | $H_2'C_2H_2''$ | |

| | Bond lengths | |
|---|---|---|
| $C_1C_2^a)$ | $C_2C_3$ | $C_1H^a)$ |
| | $ZrC_3$ | |

$^a)$　Reaction coordinates of plots in *Fig. 1*.

Further explorations of significant degrees of freedom addressed the dihedral angles $C_1C_2C_3/C_2C_3Zr$ and $H_{ag}C_1C_2/C_1C_2C_3$ which were also allowed to relax, but proved in all cases to be 180°, so that the migration of Me or H occurred strictly in plane. During the migration processes, the geometries of the fragments $L_nM = Me_4Zr$, $CpMe_2Zr$, and $CpMe_3Zr$ were optimized with respect to their interligand angles (Cp represented by the Zr-Cp centroid). All fragmental C–H and all Zr–C bond length were fixed at values taken from the relevant starting molecules 1, 2, 4, 5, 7, and 7', 8, and 9. In all calculations, the Cp ligands were kept planar with equal C–C bond distances of 1.42 Å.

REFERENCES

[1] a) T. Keii in 'Studies in Surface Science and Catalysis', Eds. T. Keii and K. Soga, Elsevier, Amsterdam, 1989, Vol. 56, p. 1, and ref. cit. therein; b) J. A. Ewen, *ibid.* 1986, Vol. 25, p. 271; c) L. L. Böhm, J. Berthold, R. Franke, V. Strobel, U. Wolfmeier, *ibid.* 1986, Vol. 25, p. 29; d) U. Zicchini, G. Cecchin, *Adv. Polym. Sci.* 1983, *51*, 101.
[2] a) P. Longo, A. Proto, A. Grassi, P. Amenendola, *Macromolecules* 1991, *24*, 4624; b) L. Cavallo, G. Guerra, M. Vacatello, P. Corradini, *ibid.* 1991, *24*, 1784; c) S. Collins, W. J. Gauthier, D. A. Holden, B. A. Kuntz, N. J. Taylor, D. G. Ward, *Organometallics* 1991, *10*, 2061; d) W. Roll, H. H. Brintzinger, B. Rieger, R. Zolk, *Angew. Chem., Int. Ed.* 1990, *29*, 279; e) P. Corradini, G. Guerra, M. Vacatello, V. Villani, *Gazz. Chim. Ital.* 1988, *118*, 173.

[3] J. C. Stevens, F. J. Timmens, D. R. Wilson, G. F. Schmidt, P. N. Nicklas, R. K. Rosen, G. W. Knight, S. Lai, Eur. Pat. Appl. 309496.0 1990.

[4] a) P. Cossee, *J. Catal.* **1964**, *3*, 80; b) E. J. Arlman, *ibid.* **1964**, *3*, 89; c) P. Cossee, E. J. Arlman, *ibid.* **1964**, *3*, 99.

[5] a) J. A. Ewen, L. Hasperlagh, M. J. Elder, J. L. Atwood, H. Zhang, H. N. Cheng, in 'Transition Metals and Organometallics as Catalysts for Olefin Polymerization', Eds. H. Sinn and W. Kaminsky, Springer, Berlin, 1988, p. 281; b) T. Keii, in 'Studies in Surface Science and Catalysis', Eds. T. Keii and K. Soga, Elsevier, Amsterdam, 1986, Vol. 25, p. 1; c) J. Eshuis, Y. Tan, J. Teuben, *J. Mol. Catal.* **1990**, *62*, 277; d) L. Resconi, F. Piemontesi, G. Franciscono, L. Albis, T. Fiorani, *J. Am. Chem. Soc.* **1992**, *114*, 1025; e) M. R. Kesti, R. M. Waymouth, *ibid.* **1992**, *114*, 3565.

[6] a) W. Keim, *Angew. Chem.* **1990**, *102*, 251; b) J. Skupinska, *Chem. Rev.* **1991**, *91*, 613; c) P. W. Jolly, G. Wilke, 'The Organic Chemistry of Nickel', Academic Press, New York, 1975; d) G. Erker, in 'Houben-Weyl, Methoden der Organischen Chemie', Thieme, Stuttgart, 1986, Bd. E 18/2, p. 843; e) W. Kaminsky, *ibid.* 1986, Bd. E 18/2, p. 894.

[7] T. W. Woo, S. I. Woo, *J. Catal.* **1991**, *132*, 68.

[8] R. Hoffmann, *Angew. Chem.* **1982**, *94*, 725.

[9] D. J. Crowther, R. F. Jordan, N. C. Baenziger, A. Verma, *Organometallics* **1990**, *9*, 2574.

[10] a) G. Erker, C. Sarter, M. Albrecht, S. Dehnicke, S. Krüger, E. Raabe, R. Schlund, R. Benn, A. Rufinska, R. Mynott, *J. Organomet. Chem.* **1990**, *382*, 89; b) R. Poli, *Chem. Rev.* **1991**, *91*, 509.

[11] a) G. Erker, *J. Organomet. Chem.* **1990**, *400*, 185; b) J. C. W. Chien, B. P. Wang, *J. Polym. Sci. Part A: Polym. Chem.* **1990**, *28*, 15; c) G. Erker, *Pure Appl. Chem.* **1992**, *64*, 393.

[12] a) A. B. Anderson, *J. Chem. Phys.* **1975**, *62*, 1187; b) D. A. Pensak, R. J. McKinney, *Inorg. Chem.* **1979**, *18*, 3407.

[13] a) A. G. Orpen, L. Brammer, F. H. Allen, O. Kennard, D. G. Watson, R. Taylor, *J. Chem. Soc., Dalton Trans.* **1989**, S1; b) H. Kawamura-Kuribayashi, N. Koga, K. Morokuma, *J. Am. Chem. Soc.* **1992**, *114*, 8687; c) G. Erker, K. Berg, K. Angermund, C. Krüger, *Organometallics* **1987**, *6*, 2620.

[14] a) H. H. Brintzinger, in 'Organic Synthesis via Organometallics', Eds. K. H. Dötz and R. W. Hoffmann, Vieweg, Braunschweig, 1990, p. 33, and ref. cit. therein; b) A. Sen, *Acc. Chem. Res.* **1988**, *21*, 421; c) H. Kawamura-Kuribayashi, N. Koga, K. Morokuma, *J. Am. Chem. Soc.* **1992**, *114*, 2359.

[15] a) G. Giundi, E. Clementi, M. E. Riuz-Vizcaya, O. Novaro, *Chem. Phys. Lett.* **1977**, *49*, 8; b) C. A. Jolly, D. S. Marynick, *J. Am. Chem. Soc.* **1989**, *111*, 7968; c) H. Fujimoto, T. Yamasaki, H. Mizutani, N. Koga, *ibid.* **1985**, *107*, 6157; d) A. C. Balzacs, K. H. Johnson, *J. Chem. Phys.* **1982**, *77*, 3148; e) O. Novara, E. Blaisten-Bajoras, E. Clementi, G. Giuchi, M. E. Ruiz-Vizcaya, *ibid.* **1978**, *68*, 2337; f) O. Novara, E. Blaisten-Barojas, *ibid.* **1978**, *68*, 2337; g) L. A. Castonguay, A. K. Rappé, *J. Am. Chem. Soc.* **1992**, *114*, 5832.

[16] a) M. Brookhart, M. L. H. Green, *J. Organomet. Chem.* **1983**, *250*, 395; b) O. Eisenstein, Y. Jean, *J. Am. Chem. Soc.* **1985**, *107*, 1177; c) S. Obara, N. Koga, K. Morokuma, *J. Organomet. Chem.* **1984**, *270*, C33; d) N. Koga, S. Obara, K. Morokuma, *J. Am. Chem. Soc.* **1984**, *106*, 4625; e) R. F. Jordan, P. K. Bradley, N. C. Baenziger, R. E. LaPointe, *ibid.* **1990**, *112*, 1289; f) A. Dedieu, *Topics Phys. Organomet. Chem.* **1985**, *1*, 1; f) M. H. Prosenc, C. Janiak, H. H. Brintzinger, *Organometallics* **1992**, *11*, 4036.

[17] a) 'Chemistry of Organozirconium and -hafnium Compounds', Eds. D. J. Cardin, M. F. Lappert, and C. L. Raston, Ellis Horwood, Chichester, 1986; b) 'Transition Metal Catalyzed Polymerizations Alkenes and Dienes', Eds. R. P. Quirk, H. L. Hsieh, G. B. Kliengensmith, and P. J. T. Tait, Part A and B, Harwood Acad. Pub., New York, 1983; c) 'Ziegler-Natta Catalysis and Polymerizations', Ed. J. Boor, Academic Press Inc., New York, 1983.

[18] a) N. Koga, K. Morokuma, *Chem. Rev.* **1991**, *91*, 823; b) N. Koga, K. Morokuma, in 'Transition Metal Hydrides', Ed. A. Dedieu, VCH Publishers, Inc., New York, 1992, p. 185–233; c) M. L. Steigerwald, W. A. Goddard, *J. Am. Chem. Soc.* **1984**, *106*, 308; d) H. Fujimoto, T. Yamasaki, H. Mizutami, N. Koga, *ibid.* **1984**, *106*, 6157; e) A. K. Rappé, *Organometallics* **1990**, *9*, 466; f) H. Rabaz, J.-Y. Saillard, R. Hoffmann, *J. Am. Chem. Soc.* **1986**, *108*, 4327; g) A. Dedieu, *Inorg. Chem.* **1981**, *20*, 2803; h) D. L. Thorn, R. Hoffmann, *J. Am. Chem. Soc.* **1978**, *100*, 2079.

[19] a) P. C. Barbe, G. Cecchin, L. Norisiti, *Adv. Polym. Sci.* **1987**, *81*, 1, and ref. cit. therein; b) J. C. W. Chien, P. L. Bres, *J. Polym. Sci. Polym. Chem. Ed.* **1986**, *24*, 2483; c) *ibid.* **1986**, *24*, 1967.

[20] a) R. F. Jordan, C. S. Bajgur, R. Willett, B. Scott, *J. Am. Chem. Soc.* **1986**, *108*, 7410; b) N. F. Wells, J. C. Huffman, K. G. Caulton, *J. Organomet. Chem.* **1981**, *21*, 1277.

[21] H. Berke, R. Hoffmann, *J. Am. Chem. Soc.* **1978**, *100*, 7224.

[22] G. Henrici-Olivé, S. Olivé, 'Coordination and Catalysis', Verlag Chemie, Weinheim, 1977, p. 146.

[23] a) K. Tatsumi, H. Yasuda, A. Nakamura, *Isr. J. Chem.* **1983**, *23*, 145; b) J. H. Howell, A. Rossi, D. Wallace, K. Haraki, R. Hoffmann, FORTICON8, QCPE Program No. 344, Indiana University, Bloomington.